Reinforcing mechanisms of natural fibers in green composites: role of fibers morphology in a PLA/hemp model system

V. Mazzanti [a], R. Pariante[b], A. Bonanno[c], O. Ruiz de Ballesteros[d], F. Mollica[a], G. Filippone[b]

[a)] Department of Engineering, Università degli Studi di Ferrara, via Saragat 1, Ferrara, Italy

[b)] DICMaPI, Università di Napoli Federico II, P. le Tecchio 80, Napoli, Italy

[c)] CNR-IMAMOTER Ferrara, Via Canal Bianco 28, Ferrara, Italy

[d)] Dipartimento di Scienze Chimiche, Università di Napoli Federico II, Via Cinthia Napoli Italy

Correspondence to: F. Mollica

Abstract

Green composites, i.e. biodegradable polymers reinforced with natural fibers, are attracting interest as potential substitutes for conventional composites based on petroleum derived plastics. The role of the inherently complex morphology of natural fibers in their reinforcing mechanisms is not completely understood and this is the topic of the present study. The selected system was poly-(lactic acid) filled with 3 and 6 wt.% of short hemp fibers. Such a low fiber amount was chosen to help visualization of the fiber – matrix interface at the scanning electron microscope. Remarkable differences in the mechanical behavior were found between composites containing fibers that were alkali treated with respect to untreated fiber filled materials, but unexpectedly it was found that the quality of the fiber – matrix interface was only marginally influenced by the alkaline treatment. Interface properties were thus not exhaustive in explaining the observed differences. On the other hand, the main difference between treated and untreated fibers was the presence, in the untreated fibers population, of a volumetrically relevant sub-population of thick fiber bundles. It was further argued that this fraction did not carry the loads transferred across the fiber-matrix interface uniformly in its cross section, thus determining a reduction in the effective fiber volume fraction. In contrast, the combined action of alkalization and the mechanical stresses during melt mixing resulted in a narrow distribution of isolated elementary fibers, which were more effective in providing higher mechanical properties, in agreement with theoretical predictions. The key message for the scientific community interested in maximizing the mechanical performances of green composites is that, besides trying to improve the quality of the fiber-matrix interface, one should also aim at minimizing the amount of fiber bundles.

Keywords: Green composites; Hemp fibers; Alkaline treatment; Poly - (lactic acid); Reinforcing mechanisms

1. Introduction

The term "biocomposite" can be applied to a wide range of materials derived wholly or in part from low environmental impact resources. Here we refer to composite materials consisting of a polymeric matrix reinforced with natural fibers [1,2]. These are gaining great consideration thanks to important advantages over traditional reinforcement, such as low environmental impact, inexpensiveness, reduced wear of the processing machineries and low density [2-5], which in turn yields excellent weight specific stiffness and strength [6]. As a consequence, major applications of biocomposites encompass many relevant industrial sectors, such as automotive, construction, and packaging [7-9]. On the other hand, natural fiber filled polymers have drawbacks such as inferior durability, difficult manufacturing, in that drying must be performed prior to processing, and poor compatibility with common polymers such as the polyolefins [10], and this can affect mechanical properties negatively [11].

Compatibilization strategies pursued to date act on the matrix side by using suitable coupling agents [10], often in the form of maleic anhydride modified polyolefins, and on the fiber side by considering chemical or physical modifications of the fibers surface [12]. The most common chemical treatment is alkalization, which is effective in removing lignin, hemicellulose, waxes and oils [5]. The resulting roughening of the surface and exposure of the hydroxyl groups of cellulose promote a better interfacial adhesion to the polar groups of the coupling agent, and this is often used to explain the improvement in mechanical properties [13].

A special class of biocomposites are the so called “green composites” [14,15]. In these materials biodegradable polymers are used as matrix, the composite is thus fully biodegradable and hence even more environmentally friendly [15,16]. Additionally, the cheap natural fibers equilibrate the relatively high cost of the biodegradable matrix, therefore green composites are rightfully attracting remarkable interest from the scientific community as well as from industry [8, 17]. Many studies have been devoted to the identification and optimization of compositions showing high performance [18-20], nevertheless green composites are relatively novel materials and there are still phenomena

that are not completely understood, only partly shared with the other biocomposites. For instance, the basic mechanisms of reinforcement certainly necessitate further targeted studies [21]. Concerning this issue, the hydrophilic nature of the biodegradable matrix (usually a polyester) allows bonding with natural fibers without the need for coupling agents that are normally necessary with hydrophobic petroleum based polymers. On the other hand, fiber chemical treatments are known to be beneficial to the mechanical properties of green composites, similarly to what happens with biocomposites. This is usually justified with the development of a fiber – matrix interface of better quality [22], but alkalization brings about many other significant morphological modifications, which are often neglected when interpreting mechanical data. The aim of this work is to consider these features explicitly and contribute to shedding additional light on the reinforcing mechanisms in alkali treated natural fiber filled green composites.

The selected system is poly-(lactic acid), briefly PLA, reinforced with short hemp fibers. PLA is arguably the most commonly used biodegradable polymer, its main advantages being that it can be obtained out of renewable resources and has good mechanical properties [23]. Hemp fibers offer relatively high mechanical properties coupled with further advantages such as fast plant growth and potentially widespread diffusion in the northern hemisphere [21].

In the present paper, low amounts of fiber loadings (3 and 6 wt.%) are considered in order to facilitate their isolation and visualization within the composites via scanning electron microscopy. Fiber morphology is studied in detail both before and after the compounding extrusion process, adopted for the dispersion within the matrix. Differences in the geometric features of alkali treated and untreated fibers will be correlated to the composites tensile properties and the detrimental role of thick fiber bundles that are present in the untreated hemp fibers population will be highlighted.

2. Materials and methods

2.1. Raw materials

Extrusion grade PLA (INGEO 2003D) was purchased by NatureWorks LLC, Minnetonka (MN) USA. Its density was 1.24 g cm^{-3} and the melt flow index was 6 g/10 min (at 210°C, 2.16 kg

weight). Raw hemp fibers (Cannabis Sativa L.) were supplied by AssoCanapa, Carmagnola (TO), Italy. They belonged to the category of bast fibers, i.e. fibers obtained from the outermost cell layers of the plant stem. After mechanical retting, the fibers were cleaned with distilled water to remove impurities and dirt before further processing.

2.2 Alkaline treatment

Once cleaned, a part of the fibers was soaked in a 5 wt.% sodium hydroxide (NaOH) solution at room temperature. Two soaking times were used (30 minutes and 24 hours) with the purpose of evaluating possible effects of treatment time. After treatment, the fibers were washed with distilled water, neutralized with 1 wt.% acetic acid solution, and dried overnight in a vacuum oven at 80°C. This treatment protocol follows closely the one reported in [20]. In this article we will refer to alkali treated fibers with TF and to untreated hemp fibers with UF.

2.3 Fourier transform infrared spectroscopy (FTIR)

FTIR was performed on TF and UF using a Thermo Scientific Nicolet iS 50 FTIR spectrometer. The spectra were collected at room temperature in the 400-4000 cm^{-1} range (4 cm^{-1} resolution). The samples were obtained by mixing the same weight of UF and TF with potassium bromide (KBr). The spectra represented an average of 40 scans corrected for the spectrum of the blank KBr.

2.4 Composites preparation

Long hemp fibers were shortened to 5-10 mm using a grinder and dried overnight together with PLA pellets at 80°C under vacuum in an oven to reduce moisture. PLA/UF and PLA/TF composite pellets were then prepared following a two-step process: first, concentrated hemp fiber masterbatches, one containing about 15 wt.% of TF and the other the same amount of UF, were obtained using a co-rotating twin screw extruder (mod. PTW 24 by Thermo Haake) equipped with a cylindrical die (1 mm diameter) and a pelletizing unit. The fibers were introduced at half the length of the extruder. Next, each of the two masterbatches was diluted with pristine PLA in a second extrusion step, for adjusting the fiber content to 3 and 6 wt.%. All extrusions were performed at a screw speed of 100 RPM with a uniform temperature distribution of 180°C along the extruder,

170°C at the die and in dry nitrogen atmosphere for minimizing hydrolytic and oxidative degradation and rehydration of the materials. The pure PLA that was used as reference was also extruded twice in the same conditions of the composites for meaningful comparison.

2.5. Tensile testing

Mechanical tests in simple tension were performed with a universal testing machine (INSTRON 4467, USA), equipped with a 500 N load cell. Dumbbell specimens (type IV of ASTM D638 standard, about 3 mm thickness) were obtained by compression molding (LP-20B, LabTech Engineering Ltd, Thailand) the dry composite pellets at 205°C and 160 bar. The procedure included a 2-minute warm up and a 3-minute stage in order to eliminate trapped air and achieve good compaction. Specimens were then cooled down to room temperature (cooling rate between -30 and -20 °C/min) while keeping compaction pressure. Simple tension tests were carried out on five specimens for each formulation at room temperature with a 2 mm/min crosshead speed. Stress was obtained by dividing the measured force by the initial cross sectional area of the sample, strain was measured using an INSTRON strain gauge extensometer (12.5 mm gauge length).

2.6 Scanning Electron Microscopy (SEM)

Morphological observations were carried out using a ZEISS Evo M15 scanning electron microscope. SEM observations were conducted on UF, TF and composite specimens. All SEM images were acquired at an accelerated voltage of 15 kV after drying and gold sputtering of the samples.

2.7 Wide Angle X-ray Diffraction (WAXD)

WAXD analyses were performed with a Panalytical Empyrean diffractometer using Cu K_α radiation (λ = 1.5418 Å) in continuous mode scan. The degree of crystallinity of PLA/UF and PLA/TF specimens (3 and 6 wt.%) was evaluated from the WAXD profiles by the ratio between the crystalline diffraction area and the total area of the diffraction profile after subtracting the amorphous halo and scaling. The WAXD profile of a PLA sample obtained by quenching the melt into cold water was used as the amorphous halo. Diffraction profiles were recorded also for raw UF

and TF and a PLA sample heated from room temperature up to 120°C at 20°C/min, and then left to crystallize in isothermal conditions. The crystallinity index (*CI*) of hemp fibers before and after alkalization was determined from the WAXD profiles by the height of the 002 reflection using the following formula [24]:

$$\mathrm{CI} = \frac{I_{002} - I_{am}}{I_{002}} \times 100 \quad (1)$$

where I_{002} is the height intensity of the 002 crystalline peak at $2\theta = 22.3°$ and I_{am} is the height of the minimum at $2\theta \approx 18°$, which represents the diffraction contribution from the amorphous material.

3. Results

3.1. Chemical and morphological effects of the alkaline treatment on hemp fibers

Fiber treatment outcome was assessed through FTIR spectroscopy, which allows to identify changes in the surface composition. The FTIR spectra of UF and TF are compared in Fig. 1.

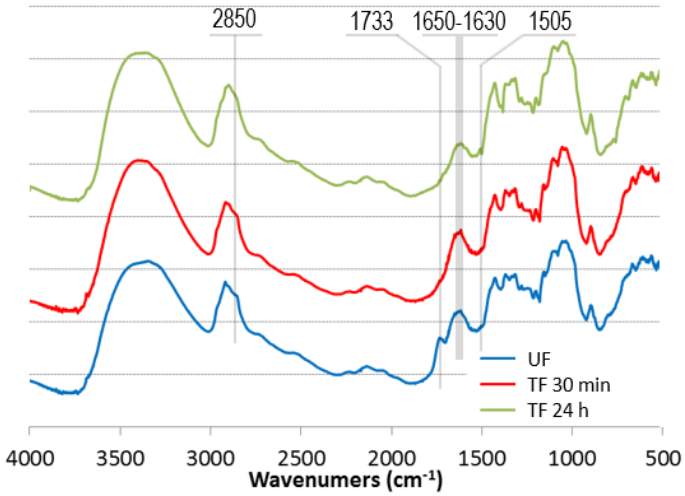

Fig. 1. FTIR spectra of the hemp fibers.

The major bands and their assignments to chemical group vibration modes can be found in [22]. The main constituent of hemp fibers is cellulose, which is the mechanically strongest component and accounts for 57÷77 wt.% of the fiber; other constituents are hemicellulose (14÷22 wt.%), lignin (4÷13 wt.%), and pectin (about 1 wt.%) [5]. The most evident effect of the alkaline treatment is the disappearance of the 1733 cm^{-1}peak, which is linked to the stretching of the C=O bonds of hemicellulose, thus the treatment decreases the hemicellulose content significantly and increases the

hydrophilic character of the hemp fibers [21,22]. The signal disappears already after the 30-minute treatment, thus the TF of this study were the ones following the short protocol.

In addition to chemical modifications of the fiber surface, alkaline treatment also alters fiber morphology. Surface roughening has received special attention, as it is considered beneficial for fiber-matrix adhesion improvement [21]. However, other non-negligible morphological alterations are induced by alkali treatment. As can be seen by comparing the SEM micrographs of Fig. 2a with Fig. 2b, the UFs appear generally thicker than the TFs.

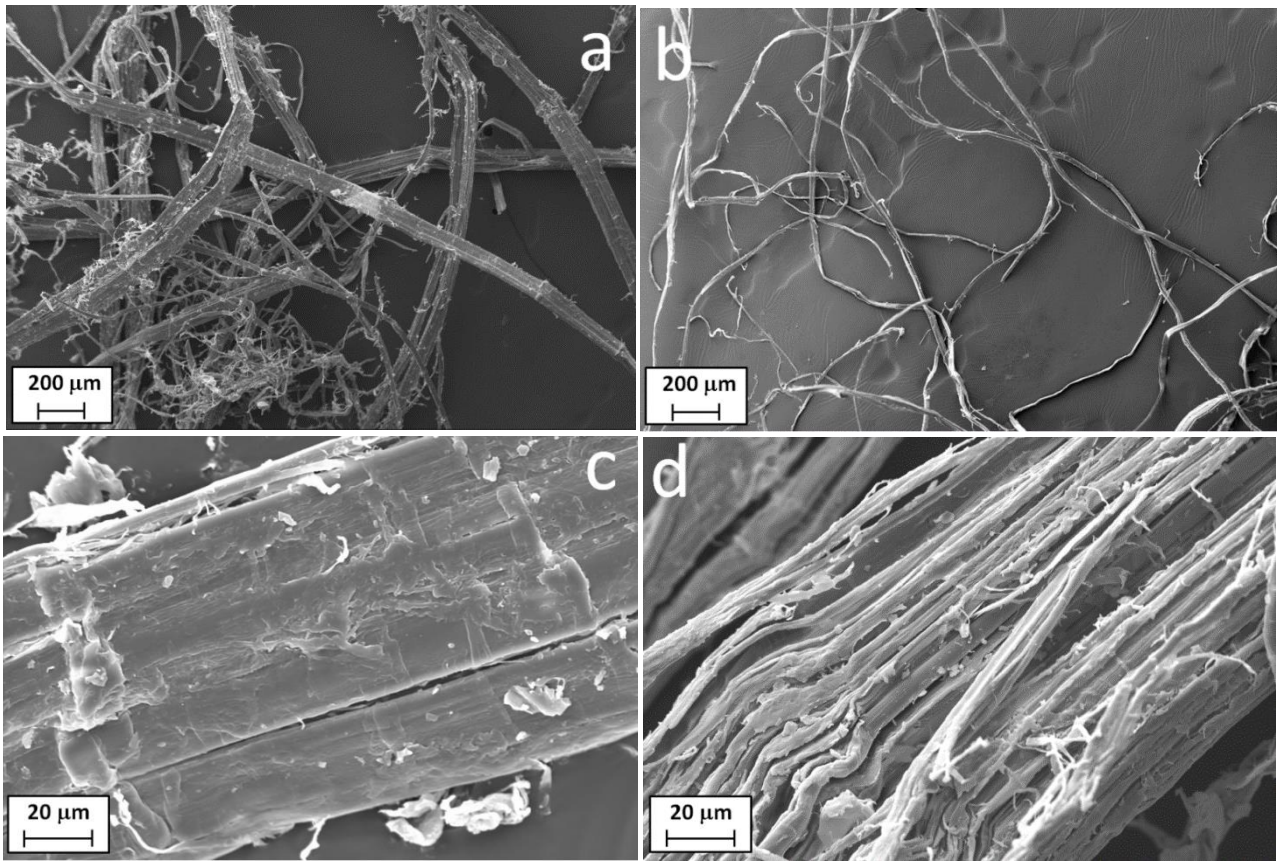

Fig. 2. SEM micrographs. (a) UF 150X, (b) TF 150X, (c) UF 2000X, (d) TF 2000X

In fact, hemp fibers consist of fiber bundles (about 100 µm diameter) made by elementary fibers glued together by an interphase composed mainly of pectins and hemicelluloses. Alkalization removes these cementing substances, unveiling the elementary fibers. This is shown in the high-magnification micrographs of Figs. 2c and 2d: UF bundles are encapsulated by a waxy layer, while the individual elementary fibers are visible in the TF bundles, thus alkalization promotes the individualization of thinner fibers.

UF and TF diameter distributions obtained by measuring about 100 different fibers are compared in Fig. 3. The UFs show a bimodal distribution, with the most frequent diameters in the ranges 20 ÷ 30 and 40 ÷ 50 µm. A similar bimodality was found in [25] and ascribed to differences in the origin of the fibers, those obtained from the outer portion of the hemp stem being thicker than the ones coming from the inner portion. Bimodality vanishes after alkalization: TFs exhibit a single-peaked diameter distribution, with most of the fibers having diameters in the range 10÷20 µm.

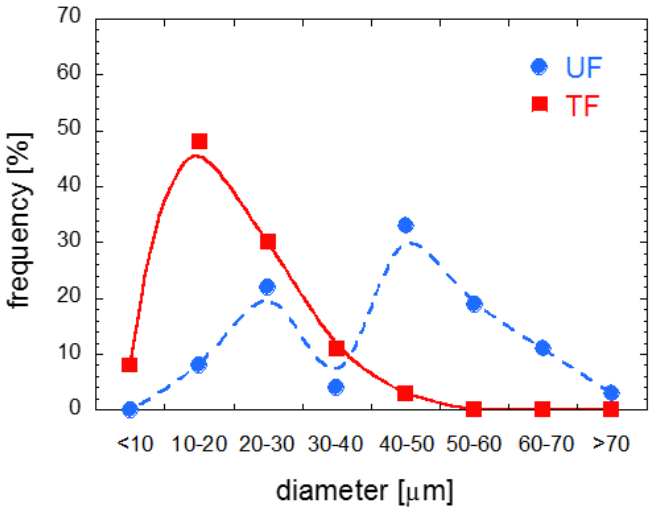

Fig. 3. Fiber diameter distributions for UF and TF.

More quantitative information is provided in Tab. 1, where two distinct average diameters, $\bar{d}_{f\text{-}thin}$ and $\bar{d}_{f\text{-}thick}$, are reported for the UF. Fiber length was impossible to measure precisely, since fibers were longer than the SEM optical range and highly entangled. In any case, fiber shortening was expected to occur during the subsequent melt compounding phase.

Table 1. Average characteristic size of the hemp fibers before and after compounding extrusion

Sample	$\bar{d}_f$ **[µm]**	$\bar{d}_{f\text{-}thin}$ (*) **[µm]**	$\bar{d}_{f\text{-}thick}$ (*) **[µm]**	$\bar{L}_f$ **[µm]**
UF	37.8 ± 15.9	18.8 ± 5.9	46.6 ± 9.6	
TF	15.7 ± 8.4			
UF post-compounding	26.9 ± 16.7	13.1 ± 7.4	44.6 ± 8.6	392 ± 92
TF post-compounding	13.5 ± 9.4			378 ± 72

(*) A fiber is considered “thin” (resp. “thick”) if d_f<30 µm (resp. d_f>30 µm).

3.2 Morphology of TF and UF after melt compounding

The effect of compounding on UF and TF morphology was studied by dissolving small pieces of 3 wt.% composites in chloroform at room temperature and filtering the fibers. SEM micrographs of UF and TF are shown in Fig. 4 and their diameter distributions are reported in Fig. 5.

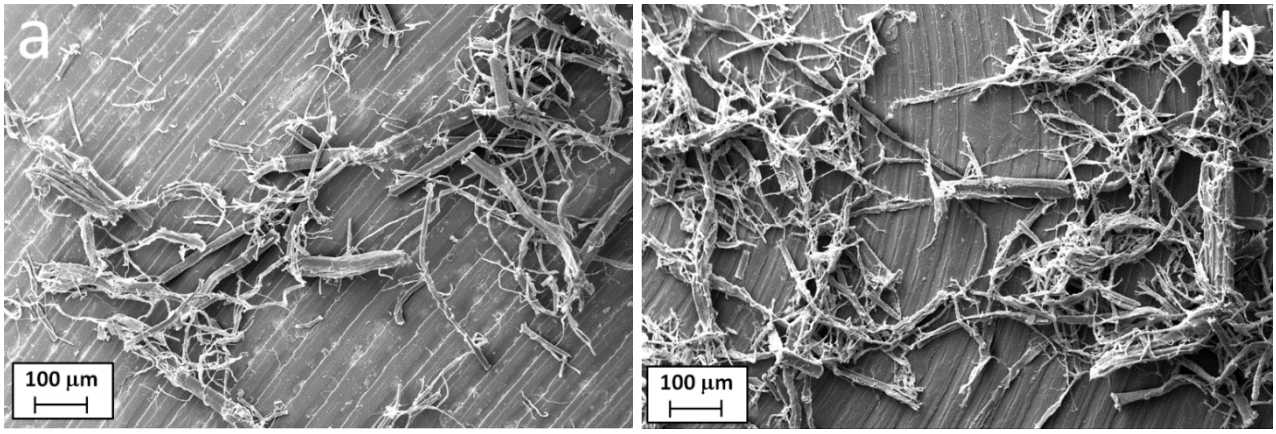

Fig. 4. SEM micrographs of UF (a) and TF (b) after melt compounding and matrix dissolution.

As already observed in Fig. 2, the UF diameters are greater than the TF ones and again it can be seen from Fig. 5 that UF and TF distributions display a double and single peak, respectively, just like the pre-extrusion distributions, which are also reported in Fig. 5. A left-shift of all distributions, though, is quite evident, especially for the thinner fraction of the UFs, thus the shearing stresses experienced during compounding extrusion promote the opening of fiber bundles.

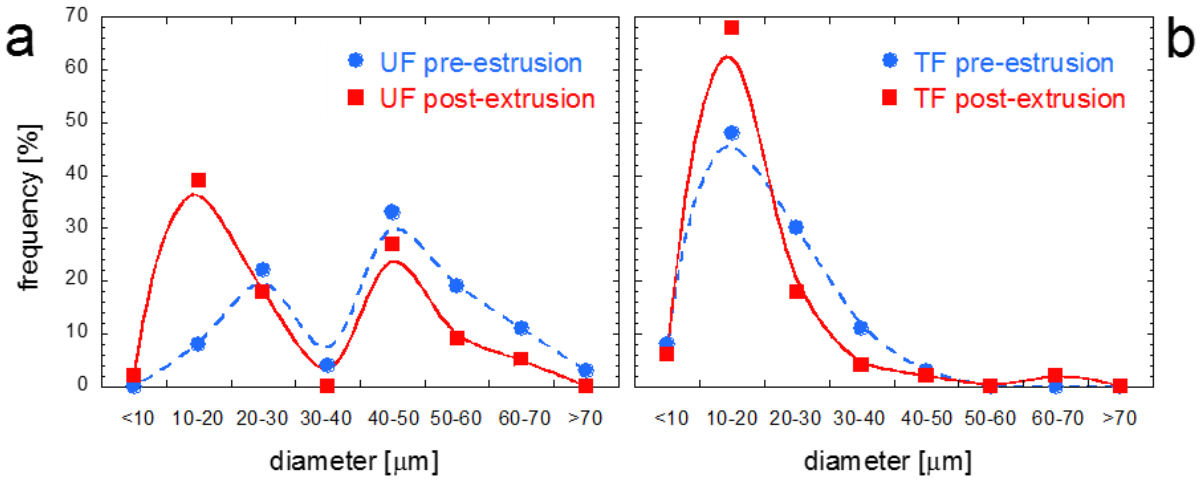

Fig. 5. Comparison of the UF (a) and TF (b) diameter distributions before and after compounding

The average characteristic size of UFs and TFs after compounding are also summarized in Tab. 1. Concerning the fiber length, $\bar{L}_f$, the measurement was restricted to the clearly identifiable fibers of the tangles in the post-compounding specimens.

3.4. Morphology of the composites interface

Representative SEM micrographs showing samples of PLA/UF and PLA/TF at 3 wt.% of fibers that were cryo-fractured in liquid nitrogen are shown in Fig. 6. The choice of low fiber content facilitates the identification of the fibers embedded in the matrix and the visualization of the interface. Several studies specifically addressed the effects of alkalization on the quality of the interface, concluding that alkali-treated hemp fibers adhere better to polar matrices such as PLA [21]. Thick fiber bundles are visible in the PLA/UF sample (Fig. 6a), whereas randomly-oriented thin fibers protrude from the fracture surface of the PLA/TF sample (Fig. 6b).

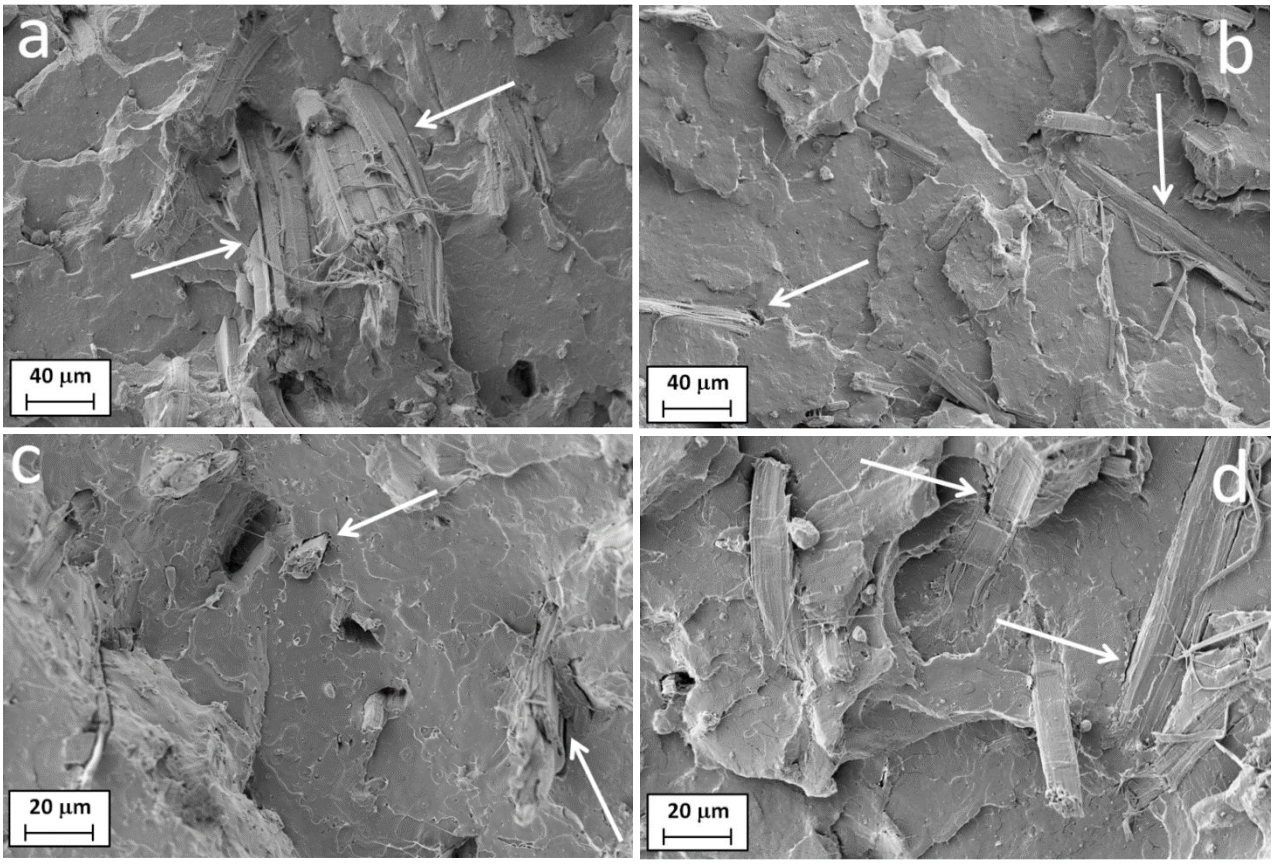

Fig. 6. SEM micrographs of the PLA/UF (a, c) and PLA/TF (b, d) composites at 3 wt.% of fibers.

Overall, the interface seems adequate in both samples, although the fiber-matrix adhesion appears to be slightly better in the PLA/TF sample due to a lower presence of pull out sites. Anyway, a closer look reveals some interfacial debonding in both materials (white arrows in Figs. 6a-d).

3.5. Assessment of crystallinity in the composite and hemp fibers samples

Although PLA crystallization characteristic times are relatively long, hemp fibers could promote heterogeneous crystallization of the matrix, thus the crystalline structure through WAXD must be considered for a correct interpretation of the mechanical properties of the composites (Fig. 7). The diffraction profiles of hemp fibers display three peaks, i.e. at 2θ = 14.7, 16, and 22.3°, corresponding to (101), (10$\bar{1}$), and (002) reflection of the monoclinic *β* form of cellulose I (assuming fiber axis along the *b* direction) [26]. In agreement with the literature [27], the alkaline treatment enhances fiber crystallinity, but the *CI* increases by a very small amount (i.e. from 87% for UF to 89% for TF). Regarding PLA, the diffraction profiles of the crystalline sample show an intense peak at 2θ = 17°, typical of the α-form of the pseudo-orthorhombic unit cell [28]. As expected, the pure PLA specimen that was obtained by rapid cooling from the melt is amorphous.

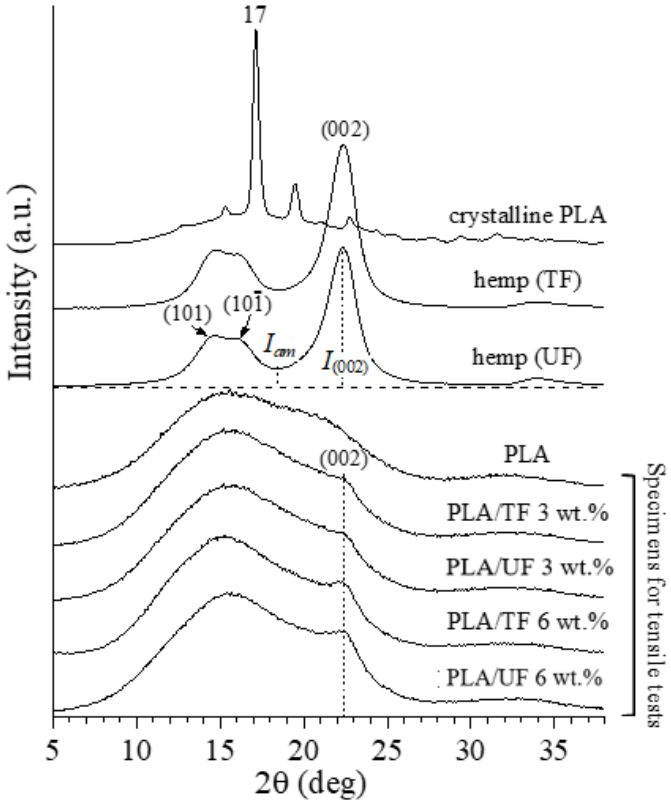

Fig. 7. X-ray diffraction profiles of hemp, neat PLA and PLA/hemp composites.

Concerning the composites, the small peaks that are visible at 2θ = 22.3° clearly originate from the cellulose contained within the hemp fibers, while the PLA matrix remains amorphous. Notice also that there is no appreciable difference between UF and TF composite specimens at the same fiber loading, while the slight increase in the peak at 2θ = 22.3°, when passing from 3 to 6 wt.%, is simply due to the increase in the hemp content.

3.6. Tensile tests

Representative stress vs. strain curves for all materials are pictured in Fig. 8, while the tensile modulus (E), strength (σ_B), and strain at break (ε_B) are summarized in Table 2.

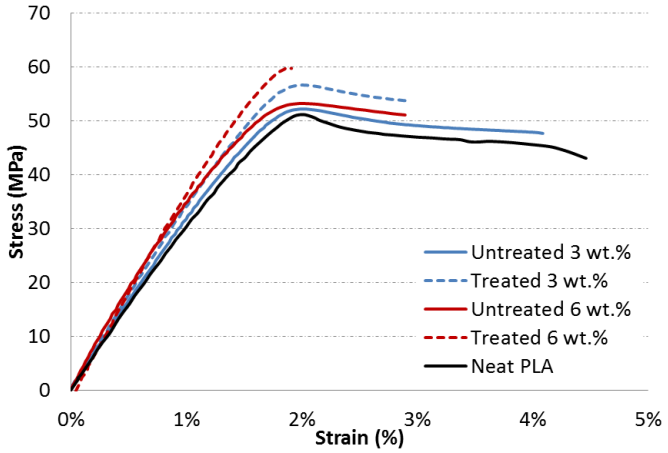

Fig. 8. Typical stress vs. strain curves for neat PLA and composites.

Table 2. Tensile modulus, strength, strain at break and differences with respect to neat PLA

Material	***E* [GPa]**	**Diff. [%]**	**σ_B [MPa]**	**Diff. [%]**	**ε_B [%]**	**Diff. [%]**
PLA	3.2 ± 0.05	0	51.4 ± 0.2	0	4.50 ± 0.1	0
PLA/UF 3 wt.%	3.4 ± 0.08	+6.25	52.5 ± 0.2	+2.1	4.06 ± 0.09	-8.9
PLA/TF 3 wt.%	3.8 ± 0.1	+18.7	55.7 ± 0.9	+8.4	3.13 ± 0.08	-29.8
PLA/UF 6 wt.%	3.8 ± 0.1	+18.7	53.2 ± 0.1	+3.5	2.90 ± 0.08	-34.9
PLA/TF 6 wt.%	4.4 ± 0.1	+37.5	59.3 ± 0.6	+15.4	1.85 ± 0.09	-58.5

The fibers cause an increase of both E and to a lesser extent σ_B. The effect is much more pronounced in PLA/TF. Concerning stiffness, the alkali treatment ensures a reinforcing effect that is higher than that induced by doubling the amount of UF (as can be seen by comparing PLA/TF at 3 wt.% with

PLA/UF at 6 wt.%). The increment in stiffness and strength is obtained at the expenses of ductility. The TF composites results reported in Tab. 2 are in overall agreement with the scientific literature, or even slightly better [20,29,30]. For instance, Sawpan et al. [20] evaluated the mechanical properties of PLA reinforced with 0, 10, 20 30 wt.% hemp fibers that were treated with various chemical treatments, including fiber alkalization. If their stiffness and strength results are interpolated at 3 and 6 wt.% fiber loadings, one can find values that are indeed very similar to the ones of the present article.

Additional information was obtained by SEM analysis of the fracture surfaces at the end of tensile tests. These specimens were of course not cryo-fractured and their micrographs are shown in Fig. 9.

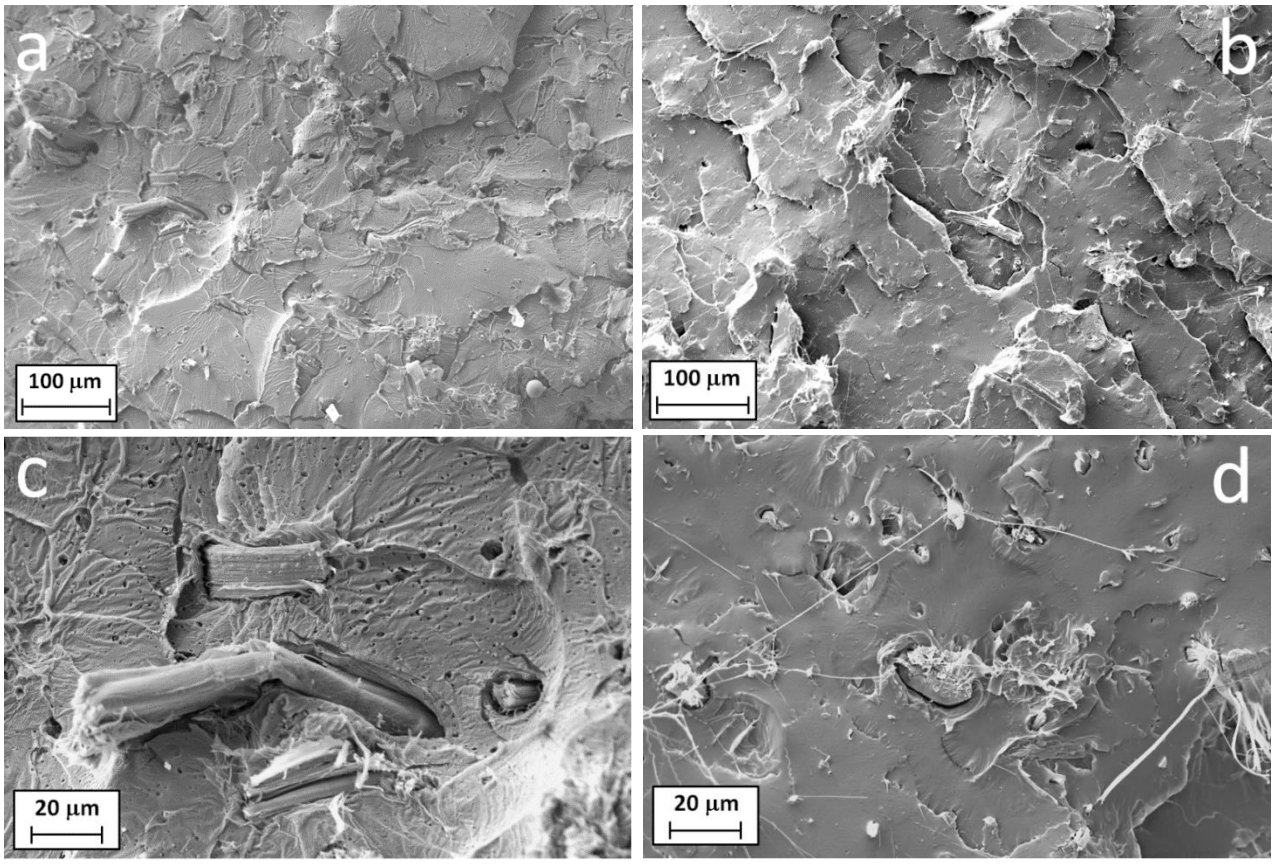

Fig. 9. Fracture surfaces of the PLA/UF (a, c) and PLA/TF (b, d) composites at 3 wt.% of fibers.

At low magnification (Figs. 9a and b) the fracture surface of the PLA/UF sample appears quite rough and this can be ascribed to matrix plasticization, which is particularly evident in the proximity of the fibers (Fig. 9c). On the other hand, the fracture surface of the PLA/TF sample is quite smooth (Fig. 9d), which is typical of brittle fracture. Notice that the different topography of

the fracture surfaces reflects the values of ε_B in Tab. 2 and Fig. 8, which indicate a slightly higher plasticization in the case of the PLA/UF samples.

4. Discussion

The most significant result of the previously described experimental investigations was the difference in mechanical properties between UF and TF composites. Alkaline treatment does not induce a crystallization increase in the PLA matrix; moreover, the increase in fiber crystallinity, while possibly determining higher properties of the TFs, is too low to explain the higher stiffness and strength of TF filled composites. Also interface properties seem to show little differences between TF and UF composites. On the other hand, fiber morphology appears to be the most significant variation, in the sense that UFs are thicker than TFs and predominantly composed of fiber bundles.

Geometrical aspects in terms of fiber aspect ratio can be introduced through the quasi-isotropic laminate theory [31,32]. This modeling approach has been recently used in [33] for the characterization of short hemp fiber filled polypropylene. In what follows we will restrict ourselves to the analysis of stiffness. This choice has been dictated in part by simplicity but also by the fact that micromechanics of strength is generally less accurate than that for stiffness.

The approximate expression for the Young's modulus for a 2-D randomly oriented short fiber reinforced lamina is [32]:

$$E_{2D} = \frac{3}{8}E_1 + \frac{5}{8}E_2 \,. \qquad (2)$$

E_1 and E_2 are the longitudinal and transverse Young's moduli of a unidirectional PLA-short hemp fiber reinforced lamina, respectively, and can be estimated through the Halpin-Tsai formulae:

$$E_i = E_m \frac{1+\xi_i \eta_i \phi}{1-\eta_i \phi}; \qquad \eta_i = \frac{E_f/E_m - 1}{E_f/E_m + \xi_i} \qquad (i = 1, 2) \qquad (3)$$

in which E_f and E_m are the Young's moduli of fibers and matrix. In the case at hand, E_m was measured and found to be equal to 3.2 GPa, while concerning the hemp fibers, typical E_f values are reported in the literature [21] and are centered around 65 GPa.

Fiber aspect ratio is taken into account by the ξ_1 parameter: for discontinuous fibers, $\xi_1 = 2\,\bar{L}_f/\bar{d}_f$, whereas ξ_2 is considered to be independent of fiber geometry and is usually taken equal to 2. The last quantity, i.e. the fiber volume fraction ϕ, can be estimated from the fiber mass fraction, w, using the following relationship:

$$\frac{1}{\phi} - 1 = \frac{\rho_f}{\rho_m}\left(\frac{1}{w} - 1\right), \tag{4}$$

where ρ_f is the density of hemp fibers (1.5 g cm^{-3} from [21]) and ρ_m the one of PLA, (1.24 g cm^{-3}). The corresponding values of ϕ for the 3 and 6 wt.% are reported in Tab. 3.

Let us now first consider PLA/TF composites. From the geometrical values of Tab. 1, it can be seen that a feasible value for ξ_1 is 56. Substituting into Eq. (3) and using the appropriate volume fractions, one obtains the values for E_1 and E_2 that are reported in Tab. 3. The values of E_{2D} can then be calculated from Eq. (2) and are also listed in Tab. 3. Such values basically coincide with the experimental values, thus PLA/TF is in agreement with [32]. If a 3D fiber distribution was assumed, the relevant analysis can be found in [34] and the estimated Young's modulus E_{3D} is given by:

$$E_{3D} = \frac{\phi}{5}E_f + \frac{1}{5}\left[\frac{(5+2\phi+\phi^2)E_f+(5+\phi)(1-\phi)E_m}{(1-\phi)E_f+(1+\phi)E_m}\right]E_m. \tag{5}$$

Interestingly, for such low fiber volume fractions, the 3D estimates are numerically equivalent to the modulus estimates based on a 2D fiber distribution, and are also reported in Tab. 3.

Table 3. Theoretical estimates of Young's moduli of the TF composites (2D Eq. 2 and 3D Eq. 5) compared with experimental values reported from Tab. 2.

Material	Φ **(%)**	E_1 **(GPa)**	E_2 **(GPa)**	E_{2D} **(GPa)**	E_{3D} **(GPa)**	E **(GPa)**
PLA/TF 3 wt.%	2.49	4.36	3.41	3.77	3.63	3.8
PLA/TF 6 wt.%	5.01	5.54	3.64	4.35	4.06	4.4

If we now turn our attention to PLA/UF composites, these have a bimodal fiber size distribution (Tab. 1 and Fig. 6), with two characteristic average diameters, i.e.13.1 μm and 44.6 μm, thus the Halpin-Tsai formulae are difficult to apply. On the other hand, if one assumed a single diameter for all fibers (i.e. a sort of equivalent diameter), one could back calculate it in order to match the

experimental values. It can be easily shown that the experimental values of *E* for both fiber loadings could be obtained using a value of ξ_1 of about 5, which for an average length of 392 μm (Tab. 1) corresponds to a fiber diameter around 150 μm. This value is clearly much too large with respect to the measured UF diameters, which are in the range 10 – 70 μm. Hence, the mechanical behavior of UF composites cannot be explained only in terms of fiber aspect ratio by the model of [32], possibly because one or more of the hypotheses at its basis are not satisfied.

As a possible explanation to justify stiffness differences between TF and UF composites, we argue that the significant presence of thick fiber bundles in the UF population (Fig. 6) deserves to be considered with more attention. In fact, the data in Fig. 6a reveal that despite the thick bundles (i.e. with d_f > 30 μm) are numerically equivalent to the thinner fibers, they account for almost 90% of the total fiber volume fraction. This indicates the relevance of this issue in order to explain the reduced mechanical reinforcement.

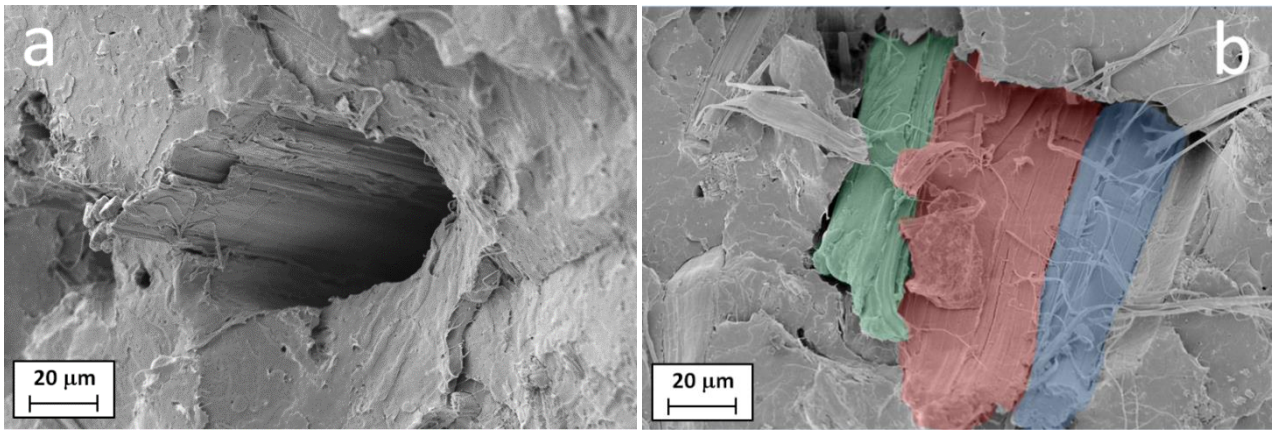

Fig. 10. Details of the fractured surfaces of PLA/UF composites: (a) hole remaining after partial pull-out of the fiber bundle; (b) detail of a thick fiber bundle with color highlighted small fibers

The raw hemp fibers that are being used are bast fibers taking the form of bundles. These are constituted by elementary fibers (Fig. 10) that are poorly bound together by non-cellulosic components, thus their shear and transverse properties are quite low. This can be seen in Fig. 10a: residual elementary fibers adhering to the polymer matrix are visible after the pull-out of a portion of the bundle, which suggests that fiber-matrix interfacial properties are higher than the interfibrillar adhesion within the fiber bundle. This type of partial pull-out can be often observed on the surface

of PLA/UF samples: another example is visible even in the central part of Fig. 6c. Low properties within the fiber bundle also emerge from visual inspection of Fig. 10b, where few smaller fibers can be distinguished.

This observation has important consequences for the mechanical properties of UF composites: fiber bundles cannot be considered isotropic materials, but rather transversely isotropic materials with weak transverse and shear properties, and this might be the reason why PLA/UF composites do not obey the theory of [32]. In order to understand the mechanical behavior of a transversely isotropic fiber reinforcing an isotropic matrix, a numerical simulation using the finite element method (FEM) implemented in the commercial finite element software ANSYS 13.0 was performed. This simulation must be intended for purely illustrative purposes.

A representative volume element in the form of an axisymmetric slice was studied in simple tension. This is composed of a rather thick fiber (in red in Fig. 11a) embedded in the matrix (in light blue in Fig. 11a). All details of the FEM simulations are reported in the supplementary material (supporting information). Two cases were studied: in the first one the fiber bundle was isotropic, while in the other one it was a transversely isotropic material, possessing low transverse and shear stiffness. Fig. 11b and c report the axial stress in the two cases. As can be seen from Fig. 11b, the isotropic bundle carries a load that is relatively uniform in its cross section, since the corresponding stress contours are almost flat. The anisotropic bundle (Fig. 11c) displays a stress distribution in which only the outer shell of the fiber bundle carries a relatively high stress (red color), while the inner portion is loaded at only about half the stress of the outer shell (green color). Matrix stress appears to be slightly higher in Fig. 11c than in Fig. 11b, accordingly.

The simulations show that both bundle types are loaded through the matrix-fiber interface by shear stresses acting along the lateral surface (the fiber ends are basically unloaded). The peripheral region of the transversely isotropic fiber bundle (i.e. its outer shell), though, is not completely effective in transmitting the load coming from the matrix-fiber interface to the bundle innermost region, since the bundle possesses low transverse and shear properties. This causes anisotropic fiber

bundles to be loaded with a non-uniform axial normal stress acting along the axis of the fiber bundles, in such a way that only the outer portion is truly able to carry external load. The net result is that the composite behaves as if it were reinforced with a smaller fiber volume fraction. The connection between weak shear properties of natural fibers and their poor tensile performance is also well explained in [35] and, at least for small fiber content, is very significant for understanding the lower tensile properties of UF composites.

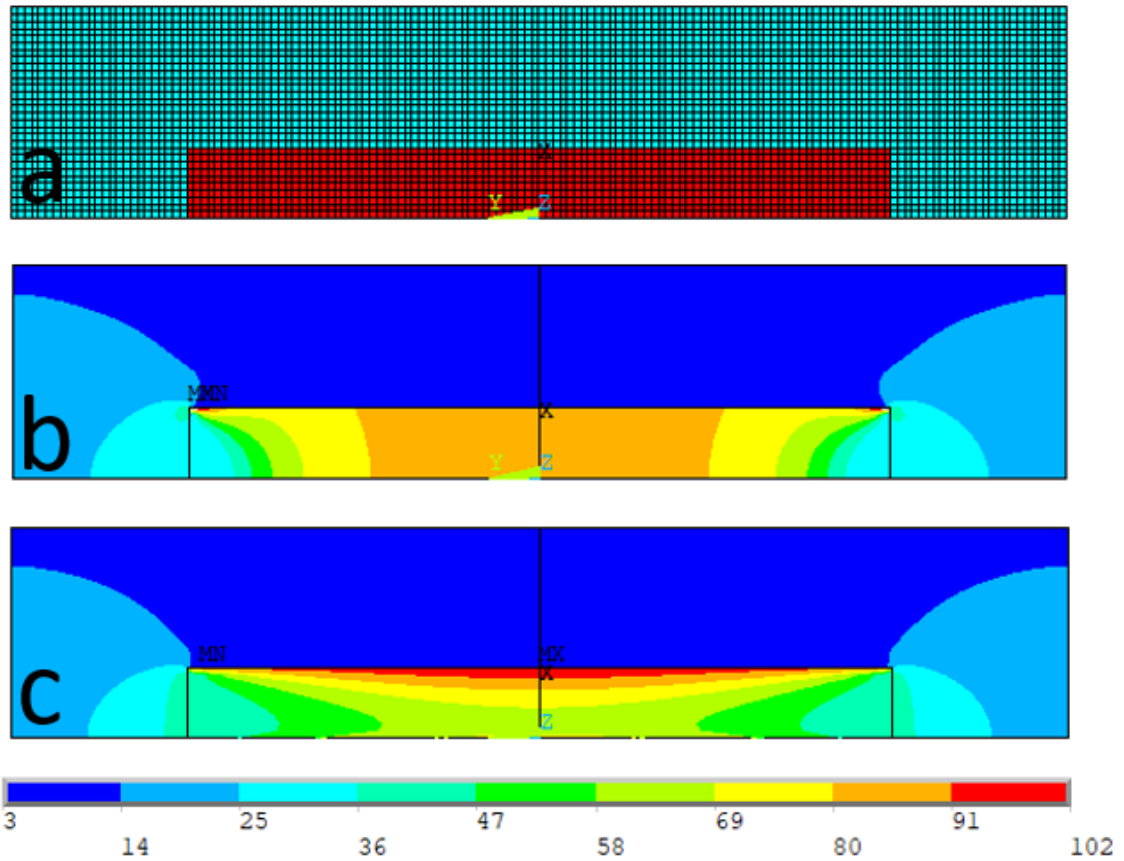

Fig. 11. RVE mesh and axial stress contour plots in MPa. (a) FEM mesh: red color for bundle, light blue for matrix; axial stress for (b) isotropic bundle and (c) for transversely isotropic bundle.

4. Conclusions

The reinforcing mechanisms in model green composites constituted by PLA containing 3 and 6 wt.% of untreated (UF) and alkali-treated (TF) hemp fibers were investigated. Tensile properties of PLA/TF composites were higher than those of analogous composites filled with UFs. SEM and WAXD analyses excluded that this could be explained with differences in fiber-matrix interfacial adhesion, fiber-induced crystallization of the matrix or changes in the crystalline structure of the

fibers promoted by alkalization. Interestingly, the SEM morphological analysis showed that the UF composites displayed a bimodal fiber distribution, with a very relevant volumetric fraction of UF consisting of rather thick fiber bundles, but the mechanical modeling with the quasi-isotropic laminate theory revealed that fiber bundles aspect ratio issues were not sufficient to justify the tensile properties differences between UF and TF green composites. On the other hand, as the UF bundles are constituted by elementary fibers that are weakly bound together, they possess low transverse and shear mechanical properties, thus the mismatch in the tensile properties of UF and TF specimens was eventually ascribed to the anisotropy of these thick fiber bundles, and their scarce effectiveness in bearing external loads was also corroborated with FEM simulations.

The beneficial effect of bundle opening and individualization of thin fibers caused by alkaline treatment coupled with shearing by compounding extrusion should not be underestimated for the enhancement of mechanical properties of bast fiber filled green composites. This renders the reinforcement less anisotropic and thus more effective in carrying loads and also allows to achieve better dispersion at equal volume fraction. Of course, the proposed mechanism is not guaranteed to hold also at higher fiber loadings, nevertheless we believe that it is an aspect that deserves further and more targeted studies.

Acknowledgments

VM and FM are deeply grateful to Mrs. Alessia Alebbi and Mr. Cesare Landini for help in the preparation and grinding of the hemp fibers.

References

[1] M.J. John, S. Thomas, Biofibres and biocomposites, Carbohyd Polym 71 (2008) 343-364.

[2] O. Adekomaya, T. Jamiru, R. Sadiku, Z. Huan, A review on the sustainability of natural fiber in matrix reinforcement – A practical perspective, J Reinf Plast Comp 35 (2016) 3-7.

[3] J. Barton-Pudik, K. Czaja, Fast-growing willow (Salix viminalis) as a filler in polyethylene composites, Comp Part B 143 (2018) 68-74.

[4] V. Mazzanti, F. Mollica, In-process measurements of flow characteristics of wood plastic composites, J Polym Environ 25 (2017) 1044-1050.

[5] X. Li, L.G. Tabil, S. Panigrahi, Chemical treatments of natural fiber for use in natural fiber-reinforced composites: a review J Polym Environ 15 (2007) 25-33.

[6] M.F. Ashby Materials and the environment: eco-informed material choice, Elsevier, 2012.

[7] E.L. Sánchez-Safont, A. Aldureid, J.M. Lagarón, J. Gámez-Pérez, L. Cabedo, Biocomposites of different lignocellulosic wastes for sustainable food packaging applications, Comp Part B 145 (2018) 215-225.

[8] G. Koronis, A. Silva, M. Fontul, Green composites: a review of adequate materials for automotive applications, Comp Part B 44 (2013) 120-127.

[9] A. Santoni, P. Bonfiglio, F. Mollica, P. Fausti, F. Pompoli, V. Mazzanti, Vibro-acoustic optimization of Wood Plastic Composite systems, Constr Build Mater 174 (2018) 730-740.

[10] A.K. Bledzki, O. Faruk, Wood fibre reinforced polypropylene composites: effect of fibre geometry and coupling agent on physico-mechanical properties, Appl Comp Mat 10 (2003) 365–379.

[11] A. Fortini, V. Mazzanti Combined effect of water uptake and temperature on wood polymer composites, J Appl Polym Sci 135 (2018) 46674.

[12] S. Kalia, B.S. Kaith, I. Kaur, Pretreatments of natural fibers and their application as reinforcing material in polymer composites - a review, Polym Eng Sci 9 (2009) 1253-1272.

[13] T. Gurunathan, S. Mohanty, S.K. Nayak, A review of the recent developments in biocomposites based on natural fibres and their application perspectives, Comp Part A 77 (2015) 1-25.

[14] M.P. Dicker, P.F. Duckworth, A.B. Baker, G. Francois, M.K. Hazzard, P.M. Weaver, Green composites: A review of material attributes and complementary applications, Comp Part A 56 (2014) 280-289.

[15] F.P. La Mantia, M. Morreale, Green composites: A brief review, Comp Part A 42 (2011) 579-588.

[16] V. Mazzanti, F. Mollica, Rheological behavior of wood flour filled poly(lactic acid): temperature and concentration dependence, Polym Comp 40 (2019) E169-E176.

[17] L. Xiao, Y. Mai, F. He, L. Yu, L. Zhang, H. Tang, G. Yang, Bio-based green composites with high performance from poly (lactic acid) and surface-modified microcrystalline cellulose, J Mater Chem 22 (2012)15732-15739.

[18] V. Fiore, L. Botta, R. Scaffaro, A. Valenza, A. Pirrotta, PLA based biocomposites reinforced with Arundo donax fillers, Comp Sci Tech 105 (2014) 110 – 117.

[19] S.Q. Yang, S.B. Bai, Q. Wang, Sustainable packaging biocomposites from polylactic acid and wheat straw: enhanced physical performance by solid state shear milling process, Comp Sci Tech 158 (2018) 34 – 42.

[20] M.A. Sawpan, K.L. Pickering, A. Fernyhough, Improvement of mechanical performance of industrial hemp fibre reinforced polylactide biocomposites, Comp Part A 42 (2011) 310-319.

[21] K.L. Pickering, M.A. Efendy, T.M. Le, A review of recent developments in natural fibre composites and their mechanical performance, Comp Part A 83 (2016) 98-112.

[22] M. Le Troëdec, D. Sedan, C. Peyratout, J.P. Bonnet, A. Smith, R. Guinebretiere, V. Gloaguen, P. Krausz, Influence of various chemical treatments on the composition and structure of hemp fibres, Comp Part A 39 (2008) 514-522.

[23] J. Lunt, Large-scale production, properties and commercial applications of polylactic acid polymers, Polym Degr Stab 59 (1998) 145-152.

[24] L. Segal, J.J. Creely, A.E. Martin, C.M. Conrad, An empirical method for estimating the degree of crystallinity of native cellulose using the X-ray diffractometer, Text Res J 29 (1962) 786-794.

[25] L. Marrot, A. Lefeuvre, B. Pontoire, A. Bourmaud, C. Baley, Analysis of the hemp fiber mechanical properties and their scattering (Fedora 17), Ind Crop Prod 51 (2013) 317-327.

[26] K.H. Meyer, L. Mish, Positions des atomes dans le nouveau modèle spatial de la cellulose, Helv Chim Acta 20 (1937) 232.

[27] S. Ouajai, R.A. Shanks, Composition, structure and thermal degradation of hemp cellulose after chemical treatments, Polym Degrad Stab 89 (2005) 327-335.

[28] P.I. Siafaka, P. Barmbalexis, D.N. Bikiaris, Novel electrospun nanofibrous matrices prepared from poly (lactic acid)/poly (butylene adipate) blends for controlled release formulations of an anti-rheumatoid agent, Eur J Pharm Sci 88 (2016) 12-25.

[29] R. Hu, J.K. Lim, Fabrication and mechanical properties of completely biodegradable hemp fiber reinforced polylactic acid composites, J Comp Mat 41 (2007) 1655-1669.

[30] M.S. Islam, K.L. Pickering, N.J. Foreman, Influence of alkali treatment on the interfacial and physico-mechanical properties of industrial hemp fibre reinforced polylactic acid composites. Comp Part A 41 (2010) 596-603.

[31] S.W. Tsai, N.J. Pagano, Invariant properties of composite materials (No. AFML-TR-67-349). AIR FORCE MATERIALS LAB WRIGHT-PATTERSON AFB OHIO, 1968.

[32] J.C. Halpin, N.J. Pagano, The laminate approximation for randomly oriented fibrous composites, J Comp Mat 3 (1969) 720-724.

[33] F. Vilaseca, R. Del Rey, R. Serrat, J. Alba, P. Mutje, F.X. Espinach, Macro and micro-mechanics behavior of stiffness in alkaline treated hemp core fibres polypropylene-based composites, Comp Part B 144 (2018) 118-125.

[34] R.M. Christensen, Mechanics of composite materials, Krieger Pub Co Malabar FL 1979.

[35] M. Fan, Characterization and performance of elementary hemp fibres: factors influencing tensile strength. BioRes 5 (2010) 2307-2322.